

Journal of Materials Chemistry A

Accepted Manuscript



This is an *Accepted Manuscript*, which has been through the Royal Society of Chemistry peer review process and has been accepted for publication.

Accepted Manuscripts are published online shortly after acceptance, before technical editing, formatting and proof reading. Using this free service, authors can make their results available to the community, in citable form, before we publish the edited article. We will replace this *Accepted Manuscript* with the edited and formatted *Advance Article* as soon as it is available.

You can find more information about *Accepted Manuscripts* in the [Information for Authors](#).

Please note that technical editing may introduce minor changes to the text and/or graphics, which may alter content. The journal's standard [Terms & Conditions](#) and the [Ethical guidelines](#) still apply. In no event shall the Royal Society of Chemistry be held responsible for any errors or omissions in this *Accepted Manuscript* or any consequences arising from the use of any information it contains.

Title

Efficient hydrogen production from formic acid using TiO₂-supported AgPd@Pd nanocatalysts

Masashi Hattori,^a Hisahiro Einaga,^b Takeshi Diao^c and Masaharu Tsuji*^a

^a *Institute for Materials Chemistry and Engineering, Kyushu University, Kasuga 816-8580, Japan. E-mail tsuji@cm.kyushu-u.ac.jp*

^b *Department of Energy and Material Sciences, Faculty of Engineering Sciences, Kyushu University, Kasuga 816-8580, Japan*

^c *International Research Center for Hydrogen Energy, Kyushu University, Motoooka, Fukuoka, 819-0395, Japan*

Abstract

We report here the significant enhancement of catalytic activity of Ag–Pd bimetallic nanocatalysts with formation of Ag–Pd catalysts having average diameter of 4.2 ± 1.5 nm on TiO₂ nanoparticles using a two-step microwave (MW)–polyol method. Data obtained using XRD and STEM–EDS indicated that Ag–Pd bimetallic nanocatalysts consisted of Ag₈₂Pd₁₈ alloy core and about 0.5 nm thick Pd shell, denoted as AgPd@Pd. The hydrogen product rate of AgPd@Pd/TiO₂ from formic acid, 16.00 ± 0.89 L g⁻¹h⁻¹, was 23 times higher than that of bare AgPd@Pd prepared under MW heating at 27 °C. It was even higher by 2–4 times than reported best Ag@Pd and CoAuPd catalysts at 20–35 °C. The apparent activation energy of the formic acid decomposition reaction using AgPd@Pd catalyst decreased from 22.8 to 7.2 kJ mol⁻¹ in the presence of TiO₂. Based on negative chemical shifts of Pd peaks in XPS data and measured activation energies, the enhancement of catalytic activity in the presence of TiO₂ was explained by the lowered energy barrier in reaction pathways because of the strong electron-donating effects of TiO₂ to Pd shells, which enhance the adsorption of formate to catalyst and dehydrogenation from formate.

Introduction

Hydrogen gas (H_2) has been anticipated as a clean energy resource that can replace fossil fuels. However, at ordinary temperatures and normal pressures, H_2 is in a gaseous state that is not compatible with storage in a small space. This constraint limits miniaturization of efficient hydrogen production systems for mobile applications. To resolve this issue, a technique must be developed to extract H_2 instantly from liquid fuels on a small scale. As such a liquid fuel, formic acid has attracted great attention because it is produced by a combination of CO_2 and H_2O with irradiation by sunlight and because it is generated as a primal product in artificial photosynthesis.¹ Some reports have described hydrogen production from the decomposition of formic acid using solid catalysts such as core–shell Au@Pd/C catalysts.^{2,3} However, for formic acid dehydrogenation, such catalysts necessitate elevated temperatures (>80 °C). Moreover, the generation of CO gas greatly reduces catalytic activity. However, hydrogen production without CO production from formic acid at room temperature has been reported recently using Ag@Pd core–shell and CoAuPd alloy catalysts.^{4,5} Although hydrogen production rates of about 4 and 8 L $g^{-1} h^{-1}$ have been achieved, higher catalytic activity without CO production is anticipated for practical application.

Reportedly, the catalytic activity of Pd nanoparticles for formic acid electrooxidation is enhanced in the presence of titanium dioxide (TiO_2).⁶ Therefore, it is expected that the catalytic activity of Ag@Pd core–shell nanocatalysts for formic acid decomposition in an aqueous solution can also be promoted by loading Ag@Pd core–shell nanocatalysts on TiO_2 . Usually, nanoparticles are loaded on an oxide semiconductor by sintering, which requires high-temperature treatment. It is difficult to load core–shell nanometals on an oxide semiconductor without alloying the core and shell metals. Based on previous results obtained for catalytic activity of Ag–Pd bimetallic system for formic acid decomposition,⁴ Ag@Pd core–shell nanocatalysts should not be alloyed because the catalytic property of the core–shell nanocatalyst is lost through alloying at high temperatures. To overcome this shortcoming, a new method must be used to synthesize core–shell nanoparticles directly on an oxide semiconductor.

In this paper, we describe a two-step microwave (MW)-polyol method used to prepare Ag–Pd bimetallic core–shell nanocatalysts directly on TiO_2 nanoparticles. Actually, TiO_2 catalysts have been widely used as photocatalysts^{7,8} and as photoelectrodes for dye-sensitized solar cells.^{9,10} For such applications, TiO_2 nanoporous substrates such as nanoparticle films and TiO_2 nanotube arrays have been developed.^{11,12} Therefore, the TiO_2 nanoporous substrates and techniques described in this work are expected to be useful for developing a practical hydrogen generation device from formic acid. For these reasons,

the trial undertaken for this study represents a reasonable and practical challenge. Results show that MW heating is more effective than conventional oil-bath heating for preparing Ag–Pd/TiO₂ nanoparticles. The hydrogen production rate of Ag–Pd/TiO₂ nanoparticles from formic acid without CO emission was higher than reported values^{4,5} at room temperature. To clarify the enhancement of catalytic activity, nanocatalysts were characterized using X-ray diffraction (XRD), transmission electron microscopy (TEM), TEM-energy dispersed X-ray spectroscopy (EDS), spherical-aberration-corrected scanning TEM (STEM), STEM-EDS, and X-ray photoelectron spectroscopy (XPS). A much higher catalytic activity with a lower apparent activation energy than that in previous reports^{4,5} has been obtained for hydrogen production from formic acid without CO emission at room temperature. Effects of TiO₂ support for the enhancement of catalytic activity were discussed on the basis of XPS data and activation energies of formic acid decomposition.

Experimental

Preparation of TiO₂ nanoparticles

TiO₂ nanoparticles were prepared by hydrolysis of titanium tetraisopropoxide (Ti(O*i*-Pr)₄) (Wako Pure Chemical Industries Ltd.) in 1,5-pentanediol (Tokyo Chemical Industry Co. Ltd.) under MW heating.¹³ 3 mmol Ti(O*i*-Pr)₄ was added to 50 ml of 1,5-pentanediol. The solution was irradiated in the MW oven (Shikoku Keisoku Kogyo K.K.; μ type, maximum output power 750 W) at 200 W for 3 min. Then 2 ml distilled water was added to this solution and irradiated at 700 W for 1 h. The temperature profile of the reagent solution is shown in Fig. S1 (ESI[†]). The solution temperature increases to 175 °C after 3 min heating at 200 W. It drops to 150 °C after injection of distilled water and increases again to about 195 °C after 6 min at 700 W and becomes nearly constant after that. For the use of TiO₂ as support of metallic nanoparticles in the next step, products were obtained by centrifuging the colloidal solution at 22,200g for 30 min. Then they were redispersed in ethylene glycol (EG) (Kishida Chemical Co. Ltd.).

Preparation of Ag–Pd/TiO₂ nanoparticles

Ag–Pd bimetallic nanocatalysts were formed on TiO₂ using a two-step heating method. First, Ag core nanoparticles were formed in the presence of TiO₂ nanoparticles. A 15 ml of EG solution containing 850 mg polyvinylpyrrolidone (PVP: average molecular weight of 40 k in terms of monomer units) (Wako Pure Chemical Industries Ltd.) and 12.26 mg AgNO₃ (Kishida Chemical Co. Ltd.) were mixed with the colloidal solution of 17.25 mg TiO₂ nanoparticles. The mixed solution was heated with MW irradiation at 50 W for 20

min under Ar bubbling. Temperature profiles of the reagent solution under MW irradiation are shown in Fig. S2 (ESI†). In the second step, 2 ml of EG containing 16.5 mg Pd(NO₃)₂ (Kishida Chemical Co. Ltd.) was added to this solution and heated with MW irradiation at 250 W or using conventional oil-bath heating for 10 min under Ar bubbling. The temperature profiles of the solutions under MW heating and oil-bath heating are shown in Fig. S3 (ESI†). Finally, the prepared samples were separated from EG solution by centrifuging the obtained colloidal solution at 22,200g for 60 min. They were dispersed in distilled water. Then, PVP was removed from the Ag–Pd/TiO₂ surface by sonication for 30 min and PVP and Ag–Pd/TiO₂ were separated by centrifuging at 22,200g for 60 min. These processes were repeated six times for removing PVP adequately. Finally, the Ag–Pd/TiO₂ particles were dispersed in distilled water.

Preparation of bare Ag–Pd nanoparticles

To examine effects of TiO₂, bare Ag–Pd bimetallic nanocatalysts were also prepared using MW heating. A 15 ml of EG solution containing 120 mg PVP and 12.26 mg AgNO₃ was heated with MW irradiation at 50 W for 20 min. Then, a 2 ml of EG containing 16.5 mg Pd(NO₃)₂ was added to this solution and heated with MW irradiation at 250 W for 10 min. The obtained Ag–Pd nanoparticles (called bare Ag–Pd (MW)) were precipitated in acetone, washed by sonication for 30 min, and then dried. These processes were repeated twice. Finally, they dispersed in distilled water. The temperature profile of the solution under MW heating was the same as that in the preparation of Ag–Pd/TiO₂ under MW heating.

Characterization of product particles

For TEM, TEM–EDS (JEM-2100F; JEOL), STEM and STEM–EDS (JEM-ARM200F; JEOL), samples were prepared by dropping colloidal solutions of the products onto Cu grids. The average sizes of product particles were determined by measuring more than 100 particles in STEM images, although much larger particles than average ones were used for the EDS analyses of single particles to obtain clear images. The XRD patterns of the samples were measured using Cu K α radiation (SmartLab; Rigaku Corp.). The XPS data of the product were measured using Al K α radiation (AXIS-165; Shimadzu Corp.). The extinction spectra of the product solutions were measured using a spectrometer (UV-3600; Shimadzu Corp.) in the ultraviolet (UV)-visible (Vis)-near infrared (NIR) region.

Hydrogen generation activity of Ag–Pd and Ag–Pd/TiO₂ nanocatalysts

The hydrogen production activity of the prepared samples was examined using the following method: total gas volume from a stirred glass tube containing 20 ml of 0.25 M aqueous formic acid and the prepared sample (metallic catalyst weight of 5.8 mg) was

measured using a gas burette. A schematic view of the measurement system is shown in Fig. S4 (ESI†). The hydrogen gas volume as production per gram of Ag–Pd catalyst per hour was calculated using equations (1) and (2).⁵

$$x_a = P_{\text{atm}}V_{\text{gas}}/RTn_{\text{FA}}, \quad (1)$$

where x_a is the conversion, P_{atm} stands for the atmospheric pressure, V_{gas} represents the generated volume of gas, R denotes the universal gas constant, T is room temperature (300 K), and n_{FA} is the mole number of formic acid.

$$R_{\text{hydrogen}} = V_{\text{gas}}/2m_{\text{metal}}t, \quad (2)$$

where R_{hydrogen} represents the initial rate of hydrogen generation when x_a reaches 20%, m_{metal} is the weight of the metallic catalyst, and t is the reaction time when x_a reaches 20%.

The H₂, CO₂, and CO gases were measured using a gas chromatograph (GC7100; J-Science): 10 ml of 1 M aqueous formic acid and the prepared sample (metallic catalyst weight of 0.97 mg) mixture were stirred for 30 min in a 110 ml glass tube filled with Ar gas. Then the atmosphere in the glass tube was measured. When the H₂, CO₂, and CO concentrations were determined using GC, data were corrected using the standard gas, which was N₂ gas containing 50,000 ppm H₂, CO₂, and CO gas.

Results and discussion

Structural characterization of TiO₂ nanoparticles

Fig. 1a shows a typical TEM image of TiO₂ particles, where monodispersed nanoparticles with average diameter of 10±2 nm are formed. Fig. 1b shows XRD patterns of the powder sample for which peaks are observed at $2\theta = 25.3^\circ$, 37.8° , 48.1° , 53.9° , and 55.1° . These peaks can be indexed to {101}, {004}, {200}, {105}, and {211} facets of anatase-type of TiO₂ (PDF 00-021-1272). No peak of rutile-type TiO₂ is observed (PDF 01-076-0325). Apparently, the products are composed solely of anatase-type of TiO₂.

Structural characterization of Ag–Pd/TiO₂ nanoparticles

Ag–Pd/TiO₂ nanoparticles were prepared by two-step heating. In the first step, AgNO₃ was reduced in EG in the presence of TiO₂ at a relatively low reaction temperature of about 130 °C under MW heating at a low power of 50 W to obtain small Ag particles with large specific surface area (Fig. S2, ESI†). In the second step, Pd(NO₃)₂ was further reduced in EG to obtain Ag–Pd bimetallic particles on TiO₂ under MW heating at 250 W or oil-bath heating. The

reaction temperature was 176–178°C (Fig. S3, ESI[†]), which was higher than that in the first step to make Ag–Pd particles adhere to a TiO₂ support strongly. Fig. 2a and 2b–d respectively portray STEM and STEM–EDS images of nanoparticles obtained from reduction of AgNO₃ in the presence of TiO₂ nanoparticles after first MW heating. Spherical Ag nanoparticles with average diameter of 2.6±1.1 nm were formed. It is noteworthy that Ag nanoparticles were not loaded on TiO₂, but are instead formed in EG solution. This fact was confirmed not only from TEM images but also from the colour of the solution, which was yellow after centrifugal separation because of formation of spherical Ag particles.

Fig. 3a–g show STEM and STEM–EDS images of products after second MW-heating for Pd shell formation. Fig. 3h shows line analysis data along the red line depicted in Fig. 3g. These images show that Ag–Pd bimetallic nanocatalysts with average diameter of 4.2±1.5 nm were loaded uniformly on TiO₂ nanoparticles and 0.5-nm-thick pure Pd shell was formed on Ag or Ag–Pd alloy core metal. The Pd/Ag atomic ratio in whole Ag–Pd bimetallic nanocatalysts was determined as 0.25±0.03 from STEM–EDS analysis. Fig. 4a–g show STEM and STEM–EDS images of products using oil-bath heating for Pd shell formation. Fig. 4h shows line analysis data along the red line depicted in Fig. 4g. These images illustrate that the shape, size, and composition of the products using oil-bath heating were almost the same as that of the products of MW-heating. The average size was 4.4±1.2 nm, the thickness of pure Pd shell was about 0.5 nm and the Pd/Ag atomic ratio in whole Ag–Pd bimetallic nanocatalysts was 0.25±0.02. On the other hand, there was a difference in loading amount of catalysts on TiO₂ support under two heating methods. In the case of oil-bath heating, there were some unloaded bare-Ag–Pd catalysts (see Fig. 4a–c) which were not observed in the products using MW-heating. Based on the data presented above, high-power MW heating at 250 W was required for strong adhesion of Ag–Pd nanoparticles to TiO₂. Under MW irradiation at high power, it is likely that Ag–Pd nanoparticles are heated locally because of skin effects of nanoparticles under MW¹⁴ so that Ag–Pd particles are strongly adhered to TiO₂ nanoparticles.

To examine crystal structures and composition of products in greater detail, we measured XRD patterns of bare Ag–Pd bimetallic nanoparticles prepared without addition of TiO₂ support (Fig. 5a) and TiO₂-supported Ag–Pd bimetallic nanoparticles (Fig. 5b). The observed XRD patterns of Ag and Pd components in bare Ag–Pd bimetallic and TiO₂-supported Ag–Pd nanoparticles are similar, indicating that the presence of TiO₂ does not affect the crystal structure of Ag–Pd bimetallic particles. Aside from TiO₂ anatase-peaks, major peaks are observed at $2\theta = 38.3^\circ$, 44.7° , 65.1° , and 78.1° in both patterns. These peaks can be indexed to {111}, {200}, {220}, and {311} facets of Ag component of fcc Ag–Pd bimetallic particles. All of these peaks shift to larger 2θ by 0.2–0.7° from those of

pure fcc Ag crystals (PDF 01-087-0720: $2\theta = 38.20^\circ, 44.40^\circ, 64.60^\circ,$ and 77.60° for {111}, {200}, {220}, and {311}, respectively) because of alloying that occurs between Ag and Pd. According to Vegard's law,¹⁵ which is known to be applicable to Ag-Pd systems,¹⁶ about $18 \pm 1\%$ of Pd atoms are dissolved in Ag-Pd particles by alloying. Weak shoulder peaks are observed at $2\theta = 40.1^\circ, 46.7^\circ, 68.1^\circ,$ and 82.1° , corresponding to the {111}, {200}, {220}, and {311} facets of Pd component of Ag-Pd bimetallic particles. Peak positions of Pd component are close to those of pure Pd atoms (PDF 01-005-0681: $2\theta = 40.12^\circ, 46.66^\circ, 68.09^\circ,$ and 82.10° , respectively, for {111}, {200}, {220}, and {311}), indicating that a major Pd component exists as pure Pd shells over Ag-rich $\text{Ag}_{82}\text{Pd}_{18}$ alloy cores. Based on XRD data, it was inferred that both Ag-Pd/TiO₂ and Ag-Pd bimetallic particles consist of $\text{Ag}_{82}\text{Pd}_{18}@Pd/TiO_2$ and $\text{Ag}_{82}\text{Pd}_{18}@Pd$ core-shell particles and that the Ag:Pd atomic ratio in AgPd cores is independent of the presence of TiO₂ nanoparticles. Consequently, when we examined the catalytic activity of $\text{Ag}_{82}\text{Pd}_{18}@Pd/TiO_2$ and $\text{Ag}_{82}\text{Pd}_{18}@Pd$ core-shell particles, only the effects of TiO₂ were found through comparison with the two data. Hereinafter, for the sake of clarity, we respectively designate $\text{Ag}_{82}\text{Pd}_{18}@Pd/TiO_2$ and $\text{Ag}_{82}\text{Pd}_{18}@Pd$ particles as AgPd@Pd/TiO₂ and AgPd@Pd.

The UV-Vis-NIR spectra of the products in each stage were measured (Fig. 6). Anatase-type TiO₂ nanoparticles showed extinction below about 350 nm and a weak tail band from approximately 350 to about 600 nm. The SPR band of spherical silver particles is observed at around 400 nm,¹⁷ whereas a long tail band without a prominent peak is found for Pd nanoparticles.¹⁸ When Ag core particles are prepared in the presence of TiO₂ particles under MW heating at 50 W, aside from the TiO₂ peak, a typical SPR band of spherical Ag nanoparticles was observed in the 350–490 nm region with a peak at about 412 nm because of the formation of free spherical Ag particles in supernatant in this stage. The extinction spectrum of AgPd@Pd/TiO₂ particles comprises a long tail band from 200 nm to 1000 nm with a shoulder peak at about 400 nm. Generally speaking, the surface plasmon resonance (SPR) band of core-shell particles reflects optical properties of shell metals.^{19,20} Consequently, the long tail band and the peak at about 400 nm can be attributed respectively to the SPR bands of Pd and Ag components of AgPd@Pd/TiO₂ particles.

To obtain chemical states of bare AgPd@Pd and AgPd@Pd/TiO₂ nanocatalysts, XPS spectra were measured (Fig. 7). For comparison, binding energies of pure Pd and Ag metals are presented as vertical dotted lines. The XPS spectra, which provide information related to chemical states within several nanometer depth from the surface of nanoparticles, show that binding energies for Pd ($3d_{5/2}$ and $3d_{3/2}$) peaks in bare AgPd@Pd shift to lower values by about 0.6 eV compared to those of pure Pd ($3d_{5/2} = 335.1$ eV, $3d_{3/2} = 340.3$ eV). Taking account of the fact that AgPd@Pd particles are covered by pure Pd shells (Fig. S5,

ESI†), these binding energy shifts originate from electron transfer from Ag to Pd because of a difference of work functions between Ag (4.7 eV) and Pd (5.1 eV). The binding energies of Ag 3d_{5/2} and Ag 3d_{3/2} in bare AgPd@Pd respectively shift to lower values by about 1.2 eV compared with those of pure Ag 3d (3d_{5/2} = 368.2 eV, 3d_{3/2} = 374.2 eV). The binding energies of Ag 3d peaks in Pd rich (> 90%) Ag–Pd alloy are known to shift to lower values by about 1 eV.²¹ It is therefore reasonable to assume that the peak shifts arise from the formation of Ag–Pd alloy around the interface of the Ag-core and Pd-shell. It is noteworthy that the binding energies of Pd (3d_{5/2} and 3d_{3/2}) and Ag (3d_{5/2} and 3d_{3/2}) in AgPd@Pd/TiO₂ (MW) both shift to lower values by about 0.9 and 0.5 eV, respectively, compared with those of bare AgPd@Pd (MW). These shifts suggest that some electrons are transferred from TiO₂ to Pd and Ag because of the large difference of the work functions between Ag (4.7 eV) or Pd (5.1 eV) and TiO₂ (4.0 eV).

Hydrogen generation activity of AgPd@Pd and AgPd@Pd/TiO₂ nanoparticles

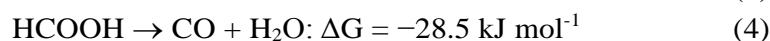
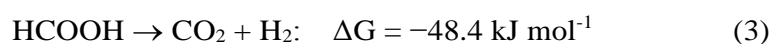
Fig. 8 presents the catalytic activities of AgPd@Pd/TiO₂ (MW), bare AgPd@Pd (MW), a mixture of bare AgPd@Pd (MW) and TiO₂, and AgPd@Pd/TiO₂ (oil) nanoparticles as counterparts for H₂ generation from formic acid decomposition. The H₂ generation rates, obtained from the relations (1) and (2), are presented in Table 1. Corresponding reported data of Ag@Pd and CoAuPd catalysts^{4,5} are given for comparison. The hydrogen production rate of the AgPd@Pd/TiO₂ (MW) sample was 16.00 L g⁻¹ h⁻¹ at room temperature (27 °C), which is about four times higher than that of Ag@Pd catalysts at 20 °C (3.67 L g⁻¹ h⁻¹)⁴ and about two times higher than that of CoAuPd catalysts at 25 °C (7.9 L g⁻¹ h⁻¹).⁵ It was about 23 times higher than that of bare AgPd@Pd (MW). The average size of bare AgPd@Pd (MW) was 4.3±1.2 nm (Fig. S5, ESI†). These sizes were nearly the same as those of AgPd@Pd/TiO₂ (MW) nanocatalysts (4.2±1.5 nm). Therefore, the much higher catalytic activity of AgPd@Pd/TiO₂ (MW) cannot be explained simply by the increase in specific surface area of nanocatalysts. It can, however, be attributed to enhancement by the assistance of TiO₂ support. To examine the catalytic activity of pure TiO₂ nanoparticles to formic acid decomposition, formic acid was mixed with TiO₂ nanoparticles without the addition of AgPd@Pd (MW) nanocatalysts. Then the gas emissions were observed. Then, no H₂ or CO₂ gas emission was observed using only TiO₂ nanoparticles. This result led us to conclude that TiO₂ does not act as a catalyst of formic acid decomposition without the presence of AgPd@Pd nanocatalysts.

The hydrogen production rate of AgPd@Pd/TiO₂ (MW) was eight times higher than that of the mixture of bare AgPd@Pd (MW) and TiO₂ nanoparticles. This result indicates that strong adhesion of AgPd@Pd (MW) and TiO₂ nanoparticles using MW heating is necessary to enhance the synergy effects between AgPd@Pd and TiO₂. Moreover, the

hydrogen production rate of AgPd@Pd/TiO₂ (MW) was 1.4 times higher than that of AgPd@Pd/TiO₂ (oil). The average size of AgPd@Pd/TiO₂ (oil) was 4.4±1.2 nm (see Fig. 4a-c). These sizes were nearly the same as those of AgPd@Pd/TiO₂ (MW) nanocatalysts (4.2±1.5 nm). This fact demonstrates that MW heating is more effective than conventional oil-bath heating for strong adhesion between AgPd@Pd nanoparticles and TiO₂ nanoparticles.

Hydrogen gas production rates were measured at various temperatures using AgPd@Pd/TiO₂ (MW) and bare AgPd@Pd (MW) catalysts (Table 1). Results show that the hydrogen product rate of bare AgPd@Pd (MW) increases more with increasing temperature from 27 to 90 °C than that of AgPd@Pd/TiO₂ (MW).

It is known that the chemical decomposition of formic acid proceeds via two main pathways, i.e., the dehydrogenation reaction to form CO₂ + H₂ and the dehydration reaction to form CO + H₂O



Although H₂ and CO₂ emissions from reaction (3) were observed, no CO emission from reaction (4) was detected using GC for AgPd@Pd/TiO₂ at 27–90 °C. Based on GC detection, the concentration of CO, which reduces the catalytic activity of AgPd@Pd/TiO₂, was estimated as <10 ppm. The apparent activation energies of reaction (3) using AgPd@Pd/TiO₂ (MW) and bare AgPd@Pd (MW) catalysts were estimated from the following relation.

$$\ln(R_{\text{hydrogen}}) = -E_a/RT + C \quad (5)$$

In that equation, R_{hydrogen} is the initial rate of hydrogen generation, E_a is the apparent activation energy, and C is a constant. The E_a values were estimated as 7.2 and 22.8 kJ mol⁻¹, respectively, for AgPd@Pd/TiO₂ (MW) and bare AgPd@Pd (MW) catalysts (see Fig. 9). The E_a value of bare AgPd@Pd (MW) catalyst is lower than those of Pd/C (53.7 kJ mol⁻¹) and Ag@Pd (30 kJ mol⁻¹).⁴ It is noteworthy that the E_a value of AgPd@Pd/TiO₂ (MW) is lower by a factor of three in comparison to that of bare AgPd@Pd (MW) catalyst. It is the lowest value ever reported in the literature.

Reaction mechanism of dehydrogenation of formic acid over AuPd@Pd/TiO₂

Based on previous DFT calculations on intermediate species,^{22,23} formate is an important intermediate in formic acid decomposition on metallic catalyts. Possible decomposition

scheme of formate on AgPd@Pd/TiO₂ is shown in Fig. 10. Decomposition starts by activating the C–H bond of formate adsorbed on the catalytic surface. In our conditions, monodentate formate (species A) transforms efficiently to more stable bidentate formate (species B), in which both oxygen atoms bind to the catalyst surface. Otherwise CO is formed through decomposition of monodentate formate (species A).⁴ Bidentate formate (species B) decomposes into CO₂* + H* (species C), where X* denotes intermediates adsorbed onto the surface. Recombination of two H* and leaving CO₂* from surface results in the formation CO₂ + H₂ gases (species D). Based on theoretical calculations on potential energy surfaces (PESs) of the formic acid decomposition reaction, the energy barrier from species B to species C is highest. It is the rate-determining step. Hu et al.²² calculated energy barriers between species B and C for Pt, Pd, Rh, and Au catalysts using {111} facets of metallic surfaces and found that a low energy barrier height for Pd is qualitatively consistent with the high hydrogen production rate from formic acid. Moreover, when they calculated PESs of Pd–Ag bilayer systems, the energy barrier of the last process becomes lower than that of pure Pd metal because migration energy of H* to the top surface of Pd decreases in the presence of Ag cores.

Present results show that the hydrogen production rate is greatly enhanced in the presence of TiO₂ for the AgPd@Pd system. Large negative chemical shifts were observed for XPS peaks of Pd (3d_{5/2,3/2}) atoms for AgPd@Pd/TiO₂ compared with those for AgPd@Pd. The work function has been regarded as an important parameter of the catalytic system for the formic acid decomposition system over M@Pd (M=Ag, Rh, Au, Ru, Pt) core–shell catalysts. The catalytic activity increases concomitantly with decrease of the work function.⁴ Therefore, the best activity has been obtained for Ag@Pd. We found here that the catalytic activity of AgPd@Pd particles are greatly enhanced in the presence of TiO₂ having a further lower work function. Larger negative chemical shifts in XPS peaks for AgPd@Pd/TiO₂ than those of bare AgPd@Pd show that more electrons were transferred from TiO₂ to Pd shells in the presence of TiO₂. Consequently, the high catalytic activity of AgPd@Pd/TiO₂ originates from a larger amount of electron transfer not only from Ag cores but also from TiO₂ support to Pd shells. Present results show that the apparent activation energy of reaction (3) using AgPd@Pd catalyst decreases by a factor of three in the presence of TiO₂. The greater degree of electron transfer from Pd layer to intermediate species A–C in the presence of TiO₂ strengthens the adsorption of formates and decreases the energy barriers of hydrogen formation and proton diffusion over catalysts.

Conclusions

Using a two-step MW-polyol method, TiO₂-supported AgPd@Pd core-shell nanoparticles having average diameter of 4.2±1.5 nm were prepared. In the first step, AgNO₃ was reduced at a low MW power of 50 W to prepare a mixture of small Ag nanoparticles and TiO₂ nanoparticles. In the second step, Ag₈₂Pd₁₈@Pd/TiO₂ particles were prepared by reducing Pd(NO₃)₂ in the presence of mixture of Ag and TiO₂ nanoparticles at a high MW power of 250 W. For comparison, AgPd@Pd/TiO₂ particles were prepared using conventional oil-bath heating. To examine effects of TiO₂, bare AgPd@Pd were synthesized under MW heating without the presence of TiO₂. The initial hydrogen formation rate of AgPd@Pd/TiO₂ from formic acid, 16.00±0.89 L g⁻¹h⁻¹, was about 23 times higher than that of bare AgPd@Pd. It was 2–4 times higher than the reported best Ag@Pd and CoAuPd catalysts at 20–35 °C. The catalytic activity of AgPd@Pd/TiO₂ particles prepared by MW heating is higher than that prepared under oil-bath heating in the second step because of stronger adhesion of AgPd@Pd catalysts on TiO₂. Consequently, MW-polyol method is a promising new mode of the loading of uniform metallic nanocatalysts on TiO₂ support adhered strongly to TiO₂. The apparent activation energy of dehydrogenation of formic acid by AgPd@Pd catalysts decreased from 22.8 kJ mol⁻¹ to 7.2 kJ mol⁻¹ in the presence of TiO₂ support. When XPS spectra of catalyst were observed, larger negative chemical shifts were observed for Pd peaks of AgPd@Pd/TiO₂ in comparison with those of bare AgPd@Pd because of electron-donating effects of TiO₂ to Pd shells. Based on the findings presented above, the marked enhancement of catalytic activity of AgPd@Pd was attributed to electron transfer from TiO₂ to AgPd@Pd catalysts, promoting C–H cleavage of formic acid over the surface of AgPd@Pd/TiO₂ nanocatalysts. In fact, CO emission, which reduces catalytic activity of AgPd@Pd/TiO, was not observed at 27–90 °C. Our method, which provides a novel preparation method for high catalytic activity of core-shell AgPd@Pd nanocatalysts on TiO₂ particles, is applicable for efficient hydrogen production systems intended for mobile applications.

Acknowledgments

We thank Mrs. Keiko Uto of our institute for her advice related to the preparation of TiO₂ nanoparticles using MW heating. This work was supported by JSPS KAKENHI (Grant nos. 25286003 and 25550056) and by the Management Expenses Grants for National University Corporations from MEXT.

Notes and references

^a Institute for Materials Chemistry and Engineering, Kyushu University, Kasuga 816-8580, Japan. E-mail tsuji@cm.kyushu-u.ac.jp

^b Department of Energy and Material Sciences, Faculty of Engineering Sciences, Kyushu University, Kasuga 816-8580, Japan

^c International Research Center for Hydrogen Energy, Kyushu University, Motoooka, Fukuoka, 819-0395, Japan

† Electronic Supplementary Information (ESI) available: [Temperature profiles of reagent solutions in each experiment and STEM and STEM–EDS images of bare AgPd@Pd nanoparticles]. See DOI: 10.1039/b000000x/

- 1 S. Sato, T. Arai, T. Morikawa, K. Uemura, T. M. Suzuki, H. Tanaka and T. Kajino, *J. Am. Chem. Soc.*, 2011, **133**, 15240–15243.
- 2 X. C. Zhou, Y. Huang, W. Xing, C. Liu, J. Liao and T. Lu, *Chem. Commun.*, 2008, 3540–3542.
- 3 Y. Huang, X. Zhou, M. Yin, C. Liu and W. Xing, *Chem. Mater.*, 2010, **22**, 5122–5128.
- 4 K. Tedsree, T. Li, S. Jones, C. W. A. Chan, K. M. K. Yu, P. A. J. Bagot, E. A. Marquis, G. D. W. Smith and S. C. E. Tsang, *Nat. Nanotechnol.*, 2011, **6**, 302–307.
- 5 Z.-L. Wang, J.-M. Yan, Y. Ping, H.-L. Wang, W.-T Zheng and Q. Jiang, *Angew. Chem. Int. Ed.*, 2013, **52**, 4406–4409.
- 6 W. Xu, Y. Gao, T. Lu, Y. Tang and B. Wu, *Catal. Lett.*, 2009, **130**, 312–317.
- 7 G. K. Kiema, M. J. Colgan and M. J. Brett, *Solar Energy Mater. Solar Cells*, 2005, **85**, 321–331.
- 8 G. K. Mor, K. Shankar, M. Paulose, O. K. Varghese and C. A. Grimes, *Nano Lett.*, 2005, **5**, 191–195.
- 9 Q. Chen and D. Xu, *J. Mater. Chem.*, 2010, **20**, 1073–1077.
- 10 O. K. Varghese, M. Paulose and C. A. Grimes, *Nature Nanotech.*, 2009, **4**, 592–597.
- 11 S. D. Burnside, V. Shklover, C. Barbé, P. Comte, F. Arendse, K. Brooks, and M. Gratzel, *Chem. Mater.*, 1998, **10**, 2419–2425.
- 12 J. M. Macak, H. Tsuchiya, L. Taveira, S. Aldabergerova and P. Schmuki, *Angew. Chem. Int. Ed.*, 2005, **44**, 7463–7465.
- 13 T. Yamamoto, Y. Wada, H. Yin, T. Sakata, H. Mori and S. Yanagida, *Chem. Lett.*, 2011, **38**, 964–965.
- 14 A. Mondal, A. Shukla, A. Upadhyaya and D. Agrawal, *Sci. Sinter.*, 2010, **42**, 169–182.
- 15 A. R. Denton and N. W. Ashcroft, *Phys. Rev. A*, 1991, **43**, 3161–3164.
- 16 L. Chen and Y. Liu, *J. Colloid Interface Sci.*, 2011, **364**, 100–106.

- 17 B. Wiley, S. H. Im, Z. H. Li, J. M. McLellan, A. Siekkinen, and Y. Xia, *J. Phys. Chem. B*, 2006, **110**, 15666–15675.
- 18 M. Tsuji, K. Ikedo, K. Uto, M. Matsunaga, Y. Yoshida and K. Takemura, *CrystEngComm*, 2013, **15**, 6553–6563.
- 19 M. B. Cortie and A. M. McDonagh, *Chem. Rev.*, 2011, **111**, 3713–3735.
- 20 M. Tsuji, K. Ikedo, M. Matsunaga and K. Uto, *CrystEngComm*, 2012, **14**, 3411–3423.
- 21 P. Steiner and S. Hufner, *Solid State Commun.*, 1981, **37**, 79–81.
- 22 A. Vittadini, A. Selloni, F. P. Rotzinger and M. Gratzel, *J. Phys. Chem. B*, 2000, **104**, 1300–1306.
- 23 C. Hu, S-W. Ting, K-Y. Chan and W. Huang, *Int. J. Hydrogen Energy*, 2012, **37**, 15956–15965.

Table 1 Hydrogen production rates from catalytic decomposition of formic acid in water at different temperatures.

Catalyst	Temperature (°C)	H ₂ gas volume (L/gh)
AgPd@Pd/TiO ₂ (MW)	27	16.00 ± 0.89
AgPd@Pd/TiO ₂ (MW)	40	16.80 ± 0.52
AgPd@Pd/TiO ₂ (MW)	60	17.89 ± 0.38
AgPd@Pd/TiO ₂ (MW)	70	21.26 ± 0.77
AgPd@Pd/TiO ₂ (MW)	90	26.73 ± 0.53
bare AgPd@Pd (MW)	27	0.71 ± 0.06
bare AgPd@Pd (MW)	40	1.19 ± 0.09
bare AgPd@Pd (MW)	60	1.98 ± 0.18
bare AgPd@Pd (MW)	70	2.54 ± 0.30
bare AgPd@Pd (MW)	90	3.34 ± 0.22
mixture (AgPd@Pd (MW) and TiO ₂)	27	2.14 ± 0.21
AgPd@Pd/TiO ₂ (oil)	27	11.76 ± 0.32
Ag@Pd (Ref. 4)	20	3.67
Ag@Pd (Ref. 4)	35	4.58
CoAuPd (Ref. 5)	25	7.9

Figure Captions

Fig. 1 TEM and XRD pattern of TiO₂ nanoparticles. (a) TEM and (b) XRD.

Fig. 2 STEM and STEM–EDS image of Ag nanoparticles synthesized using microwave heating in the presence of TiO₂ nanoparticles. (a) STEM image, (b) Ag component, (c) Ti component and (d) all components.

Fig. 3 STEM, and STEM–EDS images of AgPd@Pd/TiO₂ (MW) nanocatalysts. (a) STEM image, (b) Ag and Pd components, (c) all components, (d) STEM image, (e) Ag component, (f) Pd component, (g) Ag and Pd components and (h) line analysis data along the red line shown in Fig. 3(g).

Fig. 4 STEM, and STEM–EDS images of the AgPd@Pd nanocatalysts reduced by high-temperature (176 °C) oil-bath heating with TiO₂ nanoparticles. (a) STEM image, (b) Ag and Pd components, (c) all components, (d) STEM image, (e) Ag component, (f) Pd component, (g) Ag and Pd components, and (h) line analysis data along the red line shown in Fig. 4(g).

Fig. 5 XRD patterns of (a) bare AgPd@Pd and (b) AgPd@Pd/TiO₂ prepared using MW-polyol method.

Fig. 6 UV-Vis-NIR extinction spectra of TiO₂ nanoparticles, mixture of Ag and TiO₂ nanoparticles and AgPd@Pd/TiO₂ nanocatalysts prepared using MW heating.

Fig. 7 XPS spectra for AgPd@Pd/TiO₂ (MW) nanoparticles and bare AgPd@Pd (MW) nanoparticles, (a) Pd 3d_{3/2,5/2} and (b) Ag 3d_{3/2,5/2}.

Fig. 8 Gas generation by decomposition of formic acid (0.25 M, 20 mL) versus time in the presence of (a) AgPd@Pd/TiO₂ (MW) nanoparticles, (b) bare AgPd@Pd (MW) nanoparticles, (c) the mixture of bare AgPd@Pd (MW) and TiO₂ nanoparticles, and (d) AgPd@Pd/TiO₂ (oil) nanoparticles at 27 °C.

Fig. 9 Plots of $\ln(R_{\text{hydrogen}})$ vs $1000/T$ for AgPd@Pd/TiO₂ (MW) and bare AgPd@Pd (MW) nanocatalysts.

Fig. 10 The schematic diagram of formic acid decomposition pathways on Pd surface of AgPd@Pd/TiO₂.

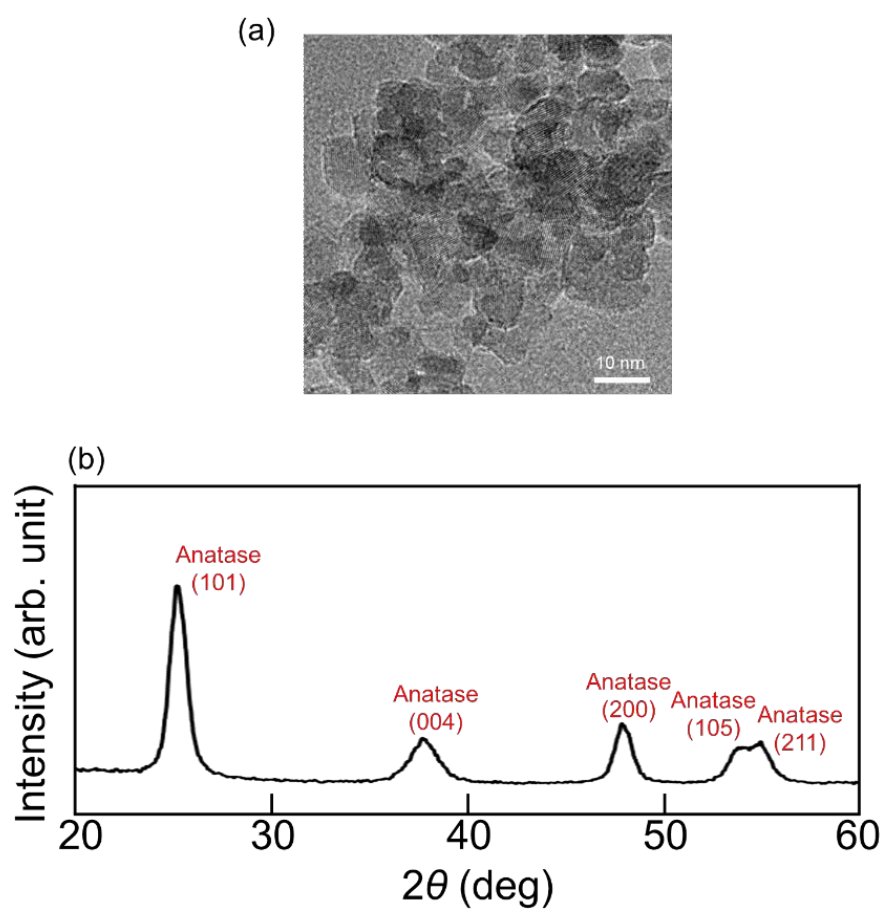


Fig. 1 TEM and XRD pattern of TiO_2 nanoparticles. (a) TEM and (b) XRD.

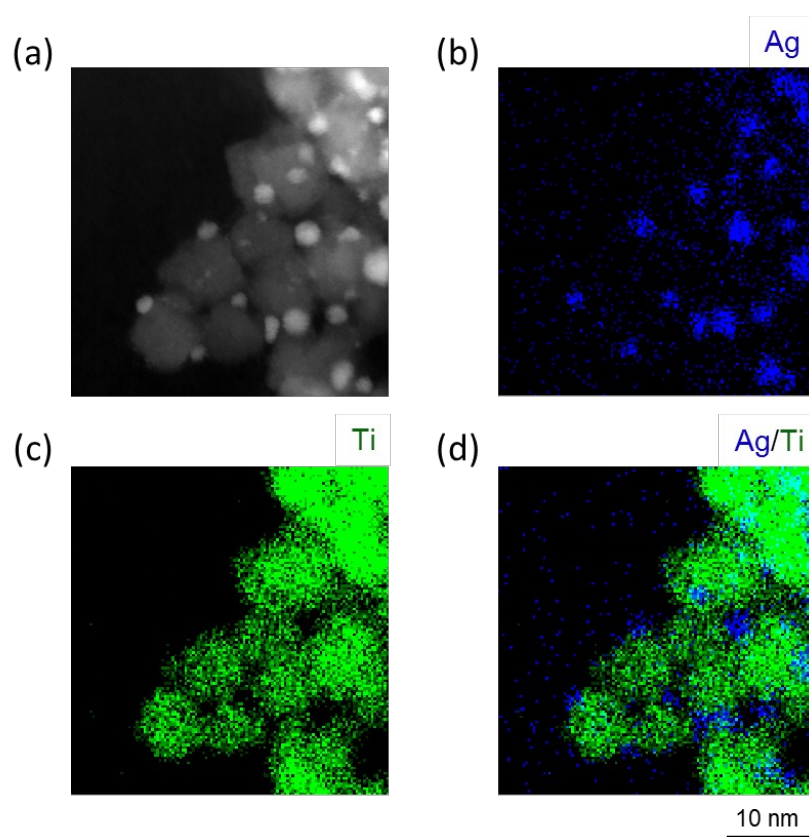


Fig. 2 STEM and STEM-EDS image of Ag nanoparticles synthesized using microwave heating in the presence of TiO₂ nanoparticles. (a) STEM image, (b) Ag component, (c) Ti component and (d) all components.

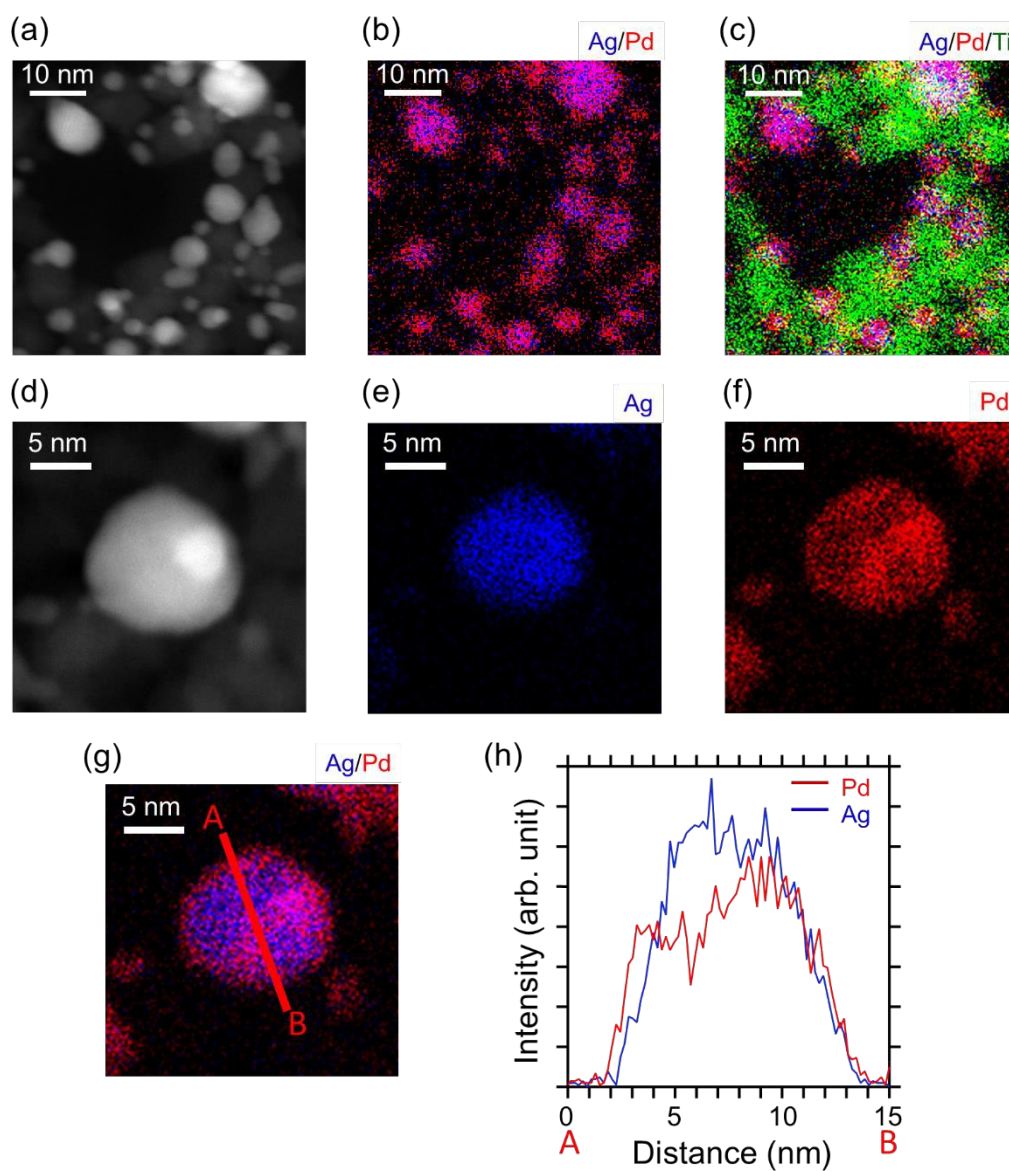


Fig. 3 STEM, and STEM-EDS images of AgPd@Pd/TiO₂ (MW) nanocatalysts. (a) STEM image, (b) Ag and Pd components, (c) all components, (d) STEM image, (e) Ag component, (f) Pd component, (g) Ag and Pd components and (h) line analysis data along the red line shown in Fig. 3(g).

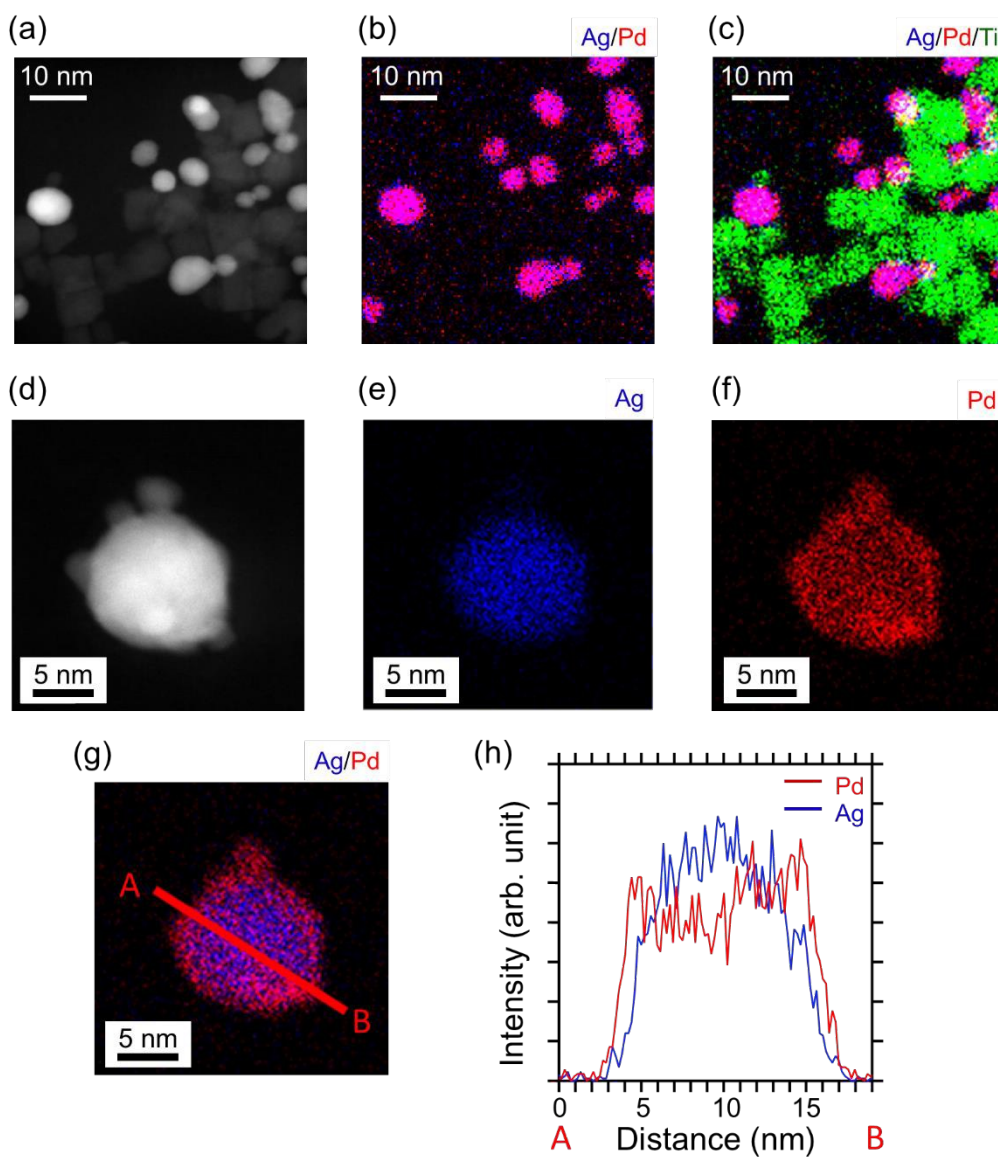


Fig 4 STEM, and STEM–EDS images of the AgPd@Pd nanocatalysts reduced by high-temperature (176 °C) oil-bath heating with TiO₂ nanoparticles. (a) STEM image, (b) Ag and Pd components, (c) all components, (d) STEM image, (e) Ag component, (f) Pd component, (g) Ag and Pd components, and (h) line analysis data along the red line shown in Fig. 4(g).

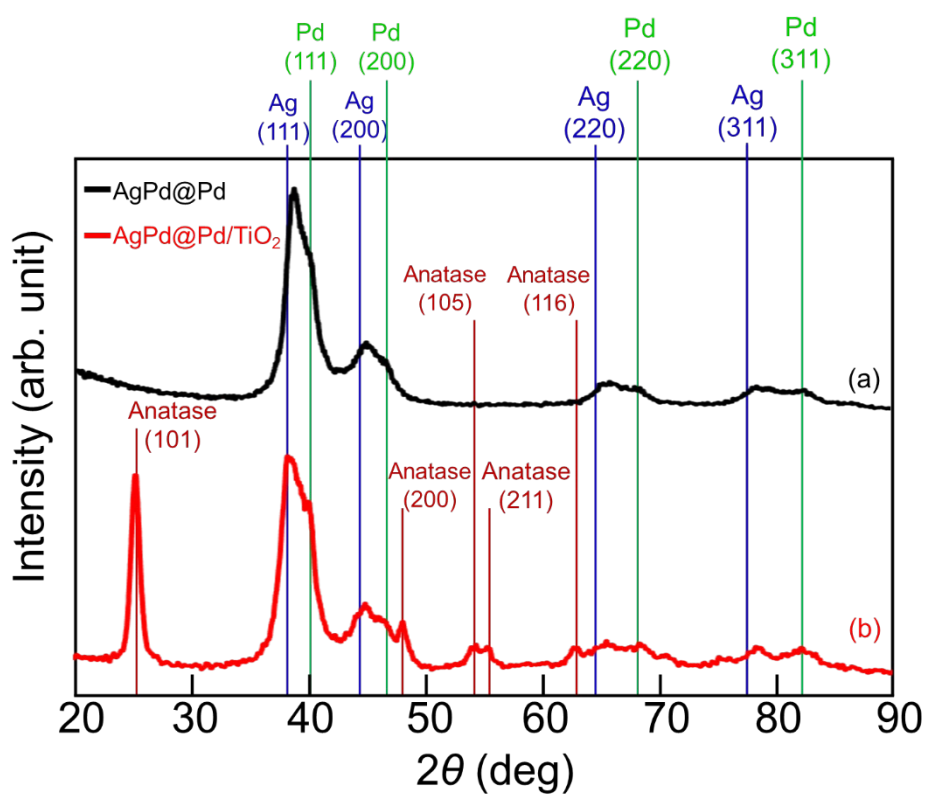


Fig. 5 XRD patterns of (a) bare AgPd@Pd and (b) AgPd@Pd/TiO₂ prepared using MW-polyol method.

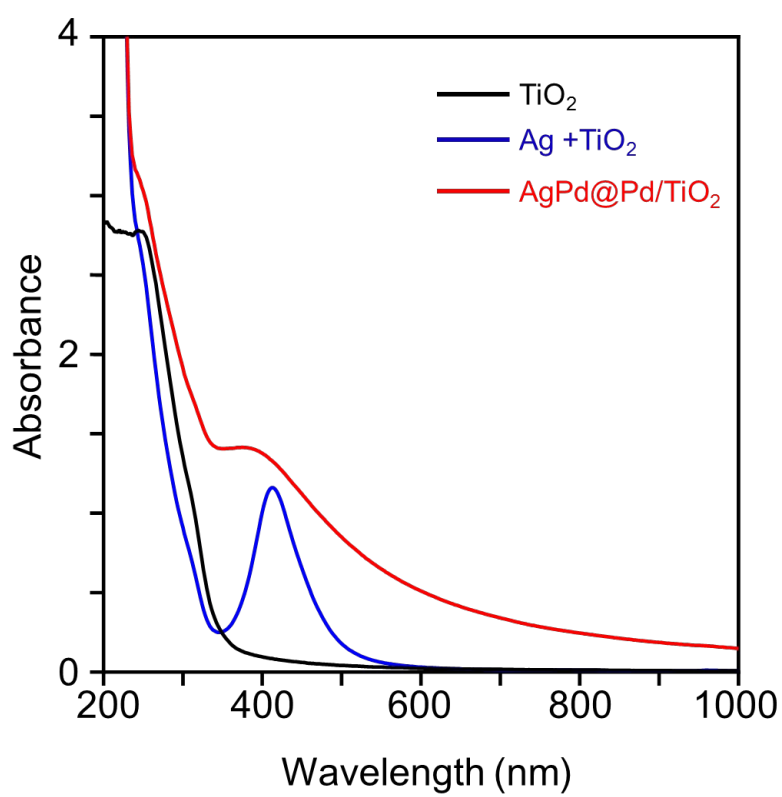


Fig. 6 UV-Vis-NIR extinction spectra of TiO₂ nanoparticles, mixture of Ag and TiO₂ nanoparticles and AgPd@Pd/TiO₂ nanaocatalysts prepared using MW heating.

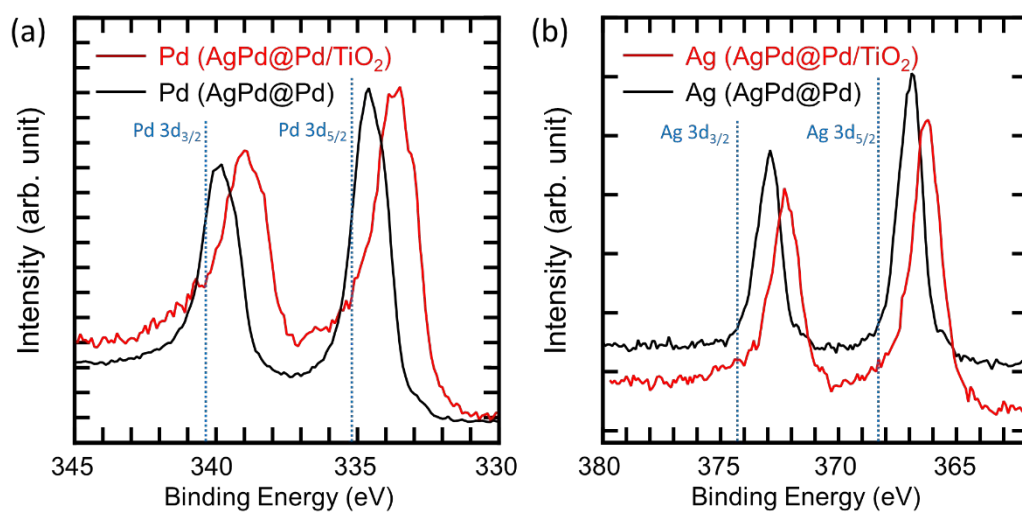


Fig. 7 XPS spectra for AgPd@Pd/TiO₂ (MW) nanoparticles and bare AgPd@Pd (MW) nanoparticles, (a) Pd 3d_{3/2,5/2} and (b) Ag 3d_{3/2,5/2}.

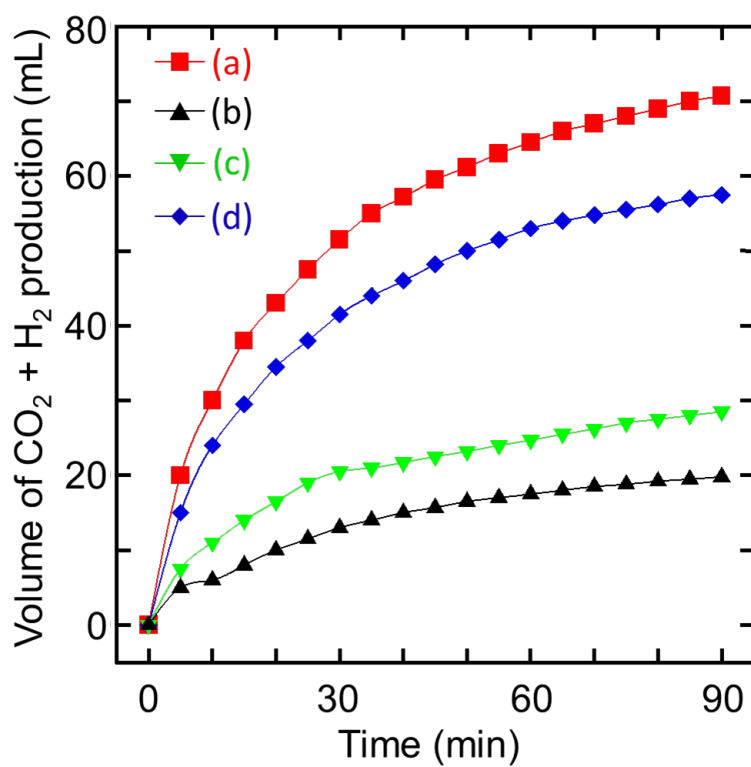


Fig. 8 Gas generation by decomposition of formic acid (0.25 M, 20 mL) versus time in the presence of (a) AgPd@Pd/TiO₂ (MW) nanoparticles, (b) bare AgPd@Pd (MW) nanoparticles, (c) the mixture of bare AgPd@Pd (MW) and TiO₂ nanoparticles, and (d) AgPd@Pd/TiO₂ (oil) nanoparticles at 27 °C.

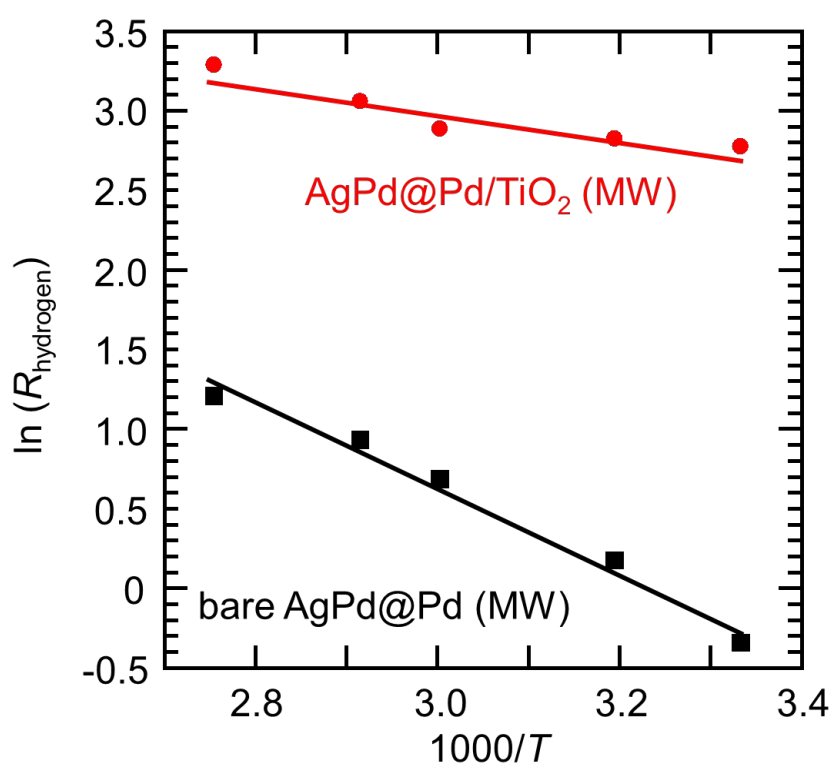


Fig. 9 Plots of $\ln(R_{\text{hydrogen}})$ vs $1000/T$ for AgPd@Pd/TiO_2 (MW) and bare AgPd@Pd (MW) nanocatalysts.

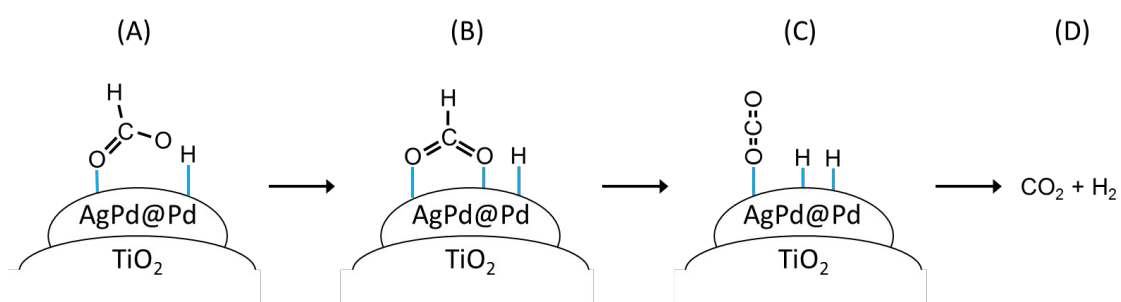
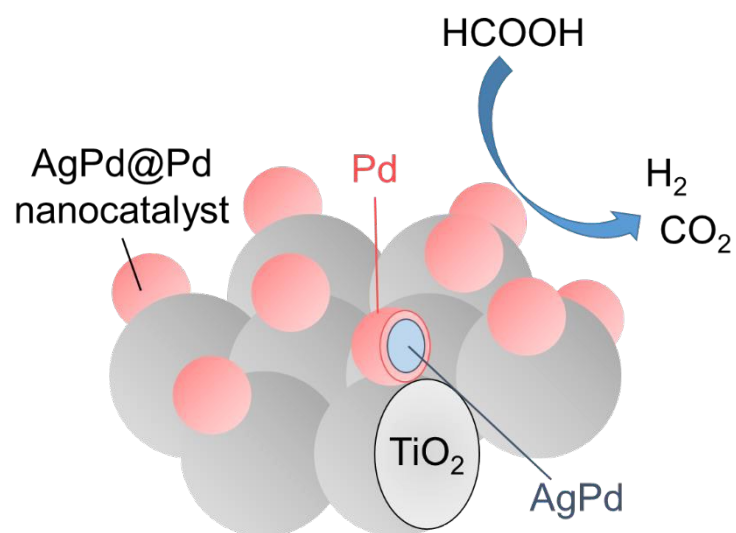


Fig. 10 The schematic diagram of formic acid decomposition pathways on Pd surface of AgPd@Pd/TiO₂.

Table of contents

AgPd@Pd core-shell nanocatalysts loaded on TiO₂ nanoparticles were fabricated using two-step microwave-polyol method for efficient hydrogen production from decomposition of formic acid.



Cover art